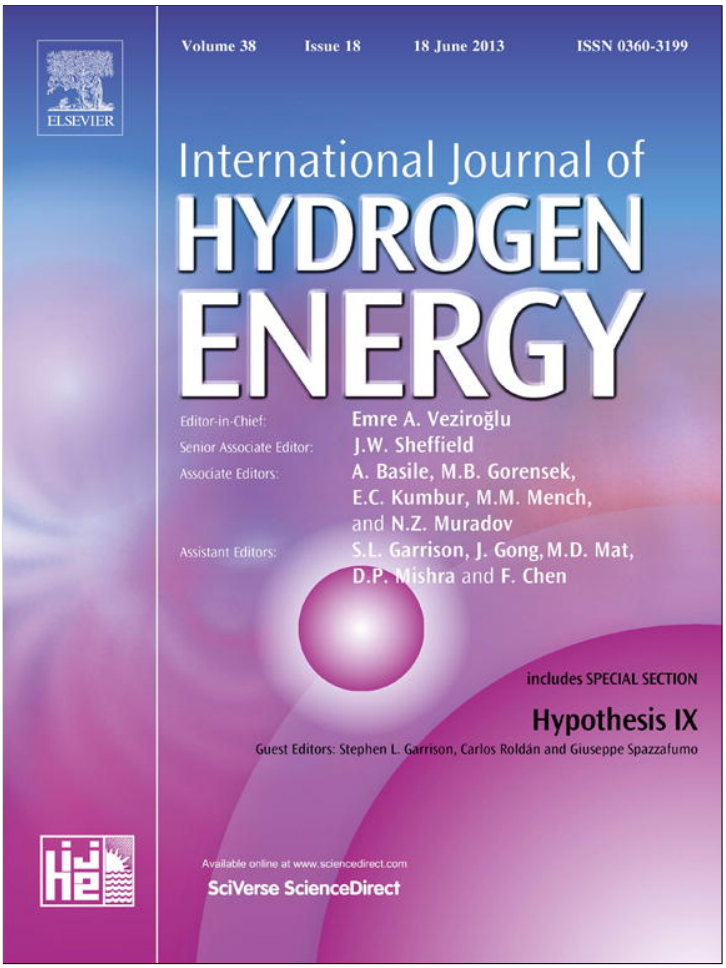

INTERNATIONAL JOURNAL OF HYDROGEN ENERGY 38 (2013) 7335–7343

Available online at www.sciencedirect.com

SciVerse ScienceDirect

journal homepage: www.elsevier.com/locate/he

Dynamic measurements of hydrogen reaction with $LaNi_{5-x}Sn_x$ alloys

E.M. Borzone [a,b], A. Baruj [a,c,*], M.V. Blanco [a,b], G.O. Meyer [a,c]

[a] Centro Atómico Bariloche, Instituto Balseiro, CNEA, U. N. Cuyo, Av. Bustillo 9500, 8400 Bariloche, Argentina
[b] Agencia Nacional de Promoción Científica y Tecnológica (ANPCyT), Argentina
[c] Consejo Nacional de Investigaciones Científicas y Técnicas (CONICET), Argentina

ARTICLE INFO

Article history:
Received 28 December 2012
Received in revised form
13 March 2013
Accepted 6 April 2013
Available online 10 May 2013

Keywords:
Hydrogen
Metal hydrides
AB5
Compression
Purification

ABSTRACT

The study focuses on the reaction between hydrogen gas and $LaNi_{5-x}Sn_x$ alloys, where $0 \leq x \leq 0.5$, in broad temperature and pressure ranges. It was performed by means of dynamic volumetric techniques using specific equipment developed at our laboratory. The substitution of Ni by Sn lowers the system equilibrium pressure and increases the hydrogen absorption reaction rate. Reaction pressures at room temperature range from 8 kPa ($x = 0.5$) to 250 kPa ($x = 0$). At 415 K the reaction pressure is within the range from 200 kPa to 4000 kPa for $x = 0.5$ and 0, respectively. The measured characteristic absorption time at 750 kPa for $LaNi_5$ is around 1 min, while it remains below 2.5 s for $LaNi_{4.5}Sn_{0.5}$. The maximum H concentration goes from 1.3 wt.% for $LaNi_5$ down to 0.95 wt.% for $LaNi_{4.5}Sn_{0.5}$. These results are useful to identify a metal system where the hydrogen interaction equilibrium properties can be tuned in a wide pressure range by choosing the chemical composition and the process temperature.

1. Introduction

Hydrides belonging to the so-called AB_5 family have been intensively studied during the last decades due to their potential for storing or purifying hydrogen. These alloys combine an extended range of equilibrium pressures with hydrogen and fast reaction kinetics at room temperature. Although their relatively low gravimetric capacity (around 1 wt.% H) in comparison with newly developed hydrogen storage materials hinders their use for mobile applications, they are still convenient for static applications. Among the AB_5 alloys, $LaNi_5$ has been the object of numerous studies due to its good hydrogen interaction properties at room temperature [1–3], its adequate resistance to cycling degradation [4–6] and to the possibility of recovering the material after degradation by means of a simple thermal treatment [4,7].

Several of $LaNi_5$ hydrogen interaction properties can be modified or adapted to a specific need by the partial substitution of its elements [8–10]. For example, it is possible to increase the equilibrium pressure by substituting part of La by Ce [11], or to achieve an improvement in electrochemical properties by replacing a fraction of La by Dy [12]. The partial substitution of Ni, on the other hand, has been reported to improve the resistance to thermal and pressure cycling degradation [3]. Ni substitutions also produce changes in the equilibrium pressure which could be useful for the development of applications based on these materials. In particular, it has been found that the substitution of small amounts of Ni by

* *Corresponding author*. Centro Atómico Bariloche, Av. Bustillo 9500, 8400 Bariloche, Argentina. Tel.: +54 294 4445278; fax: +54 294 4445299.
E-mail address: baruj@cab.cnea.gov.ar (A. Baruj).
0360-3199/$ – see front matter
http://dx.doi.org/10.1016/j.ijhydene.2013.04.035

Sn produces a steep decrease on the equilibrium pressure and improves the cycling degradation resistance of the material in comparison to $LaNi_5$ [13–16]. The resulting ternary system, $LaNi_{5-x}Sn_x$, orders in a $CaCu_5$ (P6/mmm) crystalline structure. Sn atoms replace Ni in 3g sites up to the reported solubility limit of this element at around 8 at.% Sn ($LaNi_{4.6}Sn_{0.4}$) [17,18]. Due to the fact that the atomic radius of Sn is 30% larger than that of Ni, the substitution is associated with the introduction of crystalline defects, mainly stacking faults and twins, in order to accommodate the resulting lattice distortion [19]. The formation of the full hydride, $LaNi_{5-x}Sn_xH_6$, reduces the structure symmetry to P6mm. Hydrogen atoms occupy all 3c sites and a fraction of 6e1, 6e2 y 2b sites [20]. It has been reported that the relative occupation of these sites varies between the hydride formation and hydride dissolution processes [20].

Thermodynamic data have been reported by different researchers for $LaNi_{5-x}Sn_x$ alloys in the Sn range from 0 to 0.5 at. [13,21,22]. In all cases, the results show that both the equilibrium pressure and hysteresis decrease by increasing the amount of Sn in the alloy. Luo and coworkers presented results obtained from carefully made alloys in a series of papers [14,15,23] showing the variation of equilibrium pressures and lattice parameters with Sn content and temperature. These researchers have also studied the differences between the first hydriding cycle (so-called activation cycle) and the second cycle for samples containing 0–0.5 at. Sn [23]. The results indicate that these alloys activate on their first hydriding stage. Moreover, the difference between the first and second absorption pressures strongly decreases with increasing Sn content. This difference could be related to the formation of interfaces and the entropy change due to crystal defects generation [23].

Laurencelle et al. presented absorption kinetics results for $LaNi_{4.8}Sn_{0.2}$ [16]. The activation procedure consisted, as usual, in placing a sample in contact with hydrogen while recording the pressure drop. By presenting the measurement of pressure drop versus time, these authors reported an incubation time of around 30 min. After this activation procedure, they measured reaction kinetics at different temperatures between 23 °C and 80 °C. During the absorption stage, the initial hydrogen pressure was adjusted in order to keep a constant driving force level. Under these conditions, the reported absorption kinetic coefficients are almost temperature independent. On the other hand, desorption kinetics measurements were all performed at the same pressure level (0.1 bar), leading to an increment in kinetic coefficients with the increment in temperature, which is at least partially due to the corresponding driving force increase. A study by Sato et al. [24] identified H diffusion as the limiting step for desorption kinetics. Up to the best of our knowledge, these are the only studies reporting $LaNi_{5-x}Sn_x$ alloys absorption and desorption kinetics.

We are considering the use of these alloys for an on-site hydrogen separation application. We found that, although there are reports about equilibrium pressures and heat of reaction for $LaNi_{5-x}Sn_x$ alloys, there is an important lack of data on the alloys reaction kinetics and dynamic behavior which would be necessary for designing and implementing applications. We are interested in studying the behavior of $LaNi_{5-x}Sn_x$ alloys under dynamic hydriding/dehydriding conditions, analyzing in particular possible variations of equilibrium pressures. As we mentioned before, hydrogen reaction pressures reported by previous studies correspond to quasi-static equilibrium measurements. Although this is valuable information from the point of view of thermodynamics and basic materials research, in actual applications quasi-static conditions are rarely met. It is then important to know how equilibrium parameters change under dynamic conditions. In addition, we only have information about the kinetics of hydrogen absorption and desorption for one particular $LaNi_{5-x}Sn_x$ alloy [16]. We would like to increase the existing data base, while considering a situation where a container with a given hydrogen pressure at the beginning is being depleted of gas by the hydride forming material. This situation closely resembles an actual application where an alloy is part of a hydrogen sequestration device. This paper is then aimed at providing additional experimental data on the hydrogen reaction kinetics of the $LaNi_{5-x}Sn_x$ system and further exploring its behavior under dynamic absorption/desorption conditions.

2. Experimental procedure

We have prepared $LaNi_{5-x}Sn_x$ alloys by arc melting pure La (99.9%), Ni (99.95%) and Sn (99%) several times on a water-cooled Cu crucible under Ar atmosphere. In each case, we added 5% to the Sn calculated weight in order to compensate evaporation during the melting process. The furnace chamber was first evacuated to a final pressure of 5×10^{-3} kPa and subsequently purged three times with 40 kPa Ar each. Pure elements were first joined using a low discharge voltage and later melt at full power in 7 steps. Each melting step lasted about 3 min. After each step, the alloy buttons were left to cool down and then turned upside down using a manipulator. A final melting step at low power was applied in each case in order to level the button surface. The resulting alloys, buttons weighting 10–12 g, were encapsulated in quartz under an Ar atmosphere and heat treated for 48 h at 1223 K in a muffle furnace. The encapsulated alloys were then left to slowly cool down inside the furnace. Each button was finally weighted in order to control possible material loss. In order to characterize its interaction with hydrogen, each button was mechanically broken into pieces of about 0.2 g, while exposed to air for about 30 min.

Chemical analysis was performed on samples from each alloy by means of atomic absorption spectroscopy (AAS). Table 1 presents the results, together with the alloy designation that will be used from this point on in this paper.

In order to determine structural parameters, powder samples were measured at room temperature by X-ray diffraction (XRD) using a PC controlled Philips PW3710 diffractometer in θ–2θ geometry with Cu K_α radiation at 40 kV. The receiving slit size was 0.1 mm, the step was 0.02° and the exposition time was 1 s by step. The scanned 2θ angles ranged from 10° to 90°.

Hydrogen reaction experiments on samples of about 1 g were performed using a modified Sieverts volumetric equipment designed and built at our laboratory [25]. The equipment

Table 1 – Designation, nominal composition and measured chemical composition of the studied alloys. Values, expressed in atoms per unit formula, were measured by atomic absorption spectroscopy.

Alloy designation	Nominal composition	La (at.)	Ni (at.)	Sn (at.)
Sn00	$LaNi_5$	Bal.	5.00	0.00
Sn01	$LaNi_{4.85}Sn_{0.15}$	Bal.	4.82	0.18
Sn02	$LaNi_{4.75}Sn_{0.25}$	Bal.	4.73	0.27
Sn03	$LaNi_{4.65}Sn_{0.35}$	Bal.	4.66	0.34
Sn04	$LaNi_{4.55}Sn_{0.45}$	Bal.	4.55	0.45
Sn05	$LaNi_{4.50}Sn_{0.50}$	Bal.	4.49	0.51

allows characterizing materials in the pressure range between 0 kPa and 10,000 kPa at a temperature in the range between 293 K and 823 K. The design includes a 0–20 sccm programmable mass flow controller that regulates the amount of hydrogen that enters and exits a 304L steel sample holder. The sample holder temperature is measured by means of a Pt-100 sensor placed in contact to its outer wall. Differences between the holder outer and inner temperatures were corrected by applying an experimentally determined calibration curve. In each case, measurements were started at least 20 min after the holder temperature stabilized. Experiment control and data acquisition were performed by using a dedicated PC and a computer program developed in MS Visual Basic. Dynamic pressure–composition isotherms (PCT) were measured by the mass-flow method reported by Bielmann et al. [26]. Hydrogen flow was set to 2 sccm for a sample holder free volume around 10 cm^3. Absorption kinetic measurements were performed by recording the pressure drop (of about 1 bar in the given conditions) at constant volume. During the desorption process pressure would rise, stopping the reaction. For this reason, the desorption volume was evacuated when necessary in a controlled manner. As a result, the pressure is always kept below a fixed value.

In order to characterize the materials interaction with hydrogen, we started each experiment by performing an activation procedure. This procedure consisted in placing each sample under a hydrogen pressure of 1000 kPa at 313 K for approximately 40 min. The whole set of samples containing Sn were successfully activated in this way. However, activation did not take place for the sample Sn00 ($LaNi_5$) even after 24 h under the same conditions. For this reason, we used a standard thermal cycling activation procedure for the latter sample. It consisted on one thermal cycle between 380 K and 300 K at a pressure of 6000 kPa after which the sample readily reacted with hydrogen. The morphology of powder samples after activation was observed with a Philips 515 scanning electron microscope (SEM) operating at 30 kV.

3. Experimental results and discussion

3.1. Structural parameters

XRD results indicate the presence of a single phase ordered according to a P6/mmm symmetry for all samples. The lattice parameters calculated from XRD measurements of $LaNi_{5-x}Sn_x$ alloys after heat treatment are presented in Fig. 1(a) and (b), *a* and *c* being the cell side length and height, respectively. Values reported by Wasz et al. [27] and Luo et al. [23] are also included in the figures. As it was previously found by these groups, both lattice parameters increase when the amount of Sn in the alloys is increased. Present data for parameter *a* closely agree with results from Ref. [23], these two sets of results being higher than measurements presented in Ref. [27]. In the case of parameter c, present results are slightly higher than the values previously reported by both groups of researchers [23,27], except for the $LaNi_5$ result which is similar to that measured by Luo et al. [23]. The unit cell volume linearly increases with increasing Sn content (Fig. 1(c)). In coincidence with the report from Ref. [23], present values do not deviate from the linear tendency at higher Sn contents up to $x = 0.51$, suggesting that the solubility limit has not been reached at this point. We found no significant difference between the cell parameters of samples before and after activation.

3.2. Sample activation

The activation of samples was performed in the way described in Section 2. We recorded the sample holder pressure

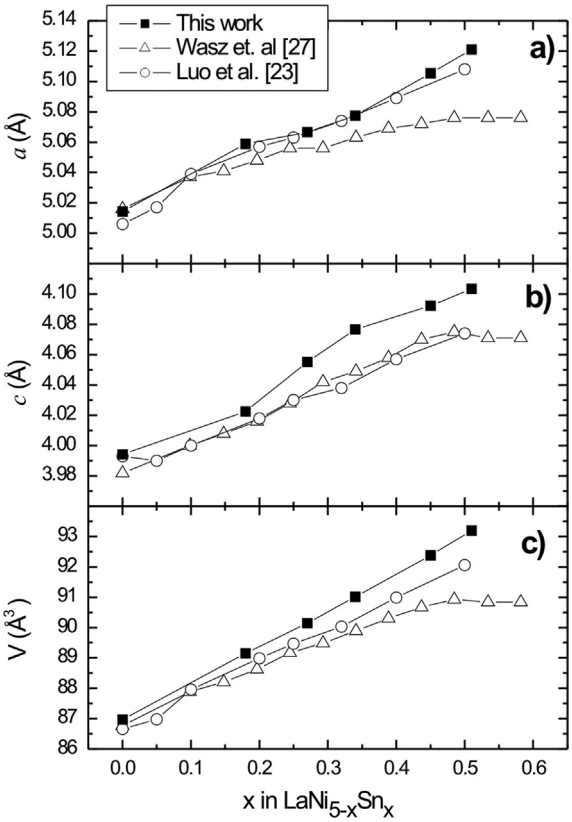

Fig. 1 – Structural parameters of $LaNi_{5-x}Sn_x$ alloys calculated from XRD measurements as a function of Sn content. Results from Wasz et al. [27] and Luo et al. [23] are included. The cell geometry is hexagonal. (a) Lattice parameter *a*, corresponding to the hexagonal cell side length. (b) Lattice parameter c, corresponding to the cell height. (c) Volume per unit cell.

evolution as a function of time during the activation procedure. Fig. 2(a) shows the activation curves for samples containing Sn. In all cases, activation took place in two stages. In the first one, immediately after the samples were placed under activation conditions, there is an incubation process. During this stage the pressure remained stable and hydrogen intake by the samples was not detected. After this incubation stage, samples started absorbing hydrogen up to a point where the pressure stabilizes again. The observed trend during this second stage is to decrease the total amount of absorbed hydrogen with the increment in Sn content.

Although the incubation process was observed in all of the samples under study, it is difficult to precisely establish an incubation time for each alloy because there are important variations from sample to sample, even for the same alloy. We observed a loose correlation indicating that an increase in the substitution level leads to a decrease in the incubation time, as illustrated in Fig. 2(a). However, the incubation times shown in the figure should be regarded with caution because they strongly depended on each sample surface conditions at the beginning of the experiments. These conditions depend on a number of factors such as air exposure time before activation [28].

After a sample was subjected to the activation process described above, the incubation stage was no longer observed. As an example of this behavior, Fig. 2(b) shows hydrogen absorption stages during and after activation for sample Sn04. While the incubation process roughly takes 300 s during the activation cycle, hydrogen intake occurs immediately during subsequent cycles. It is also remarkable that the sample reaches the same final hydrogen concentration after these two absorption stages, indicating that the sample reaches its full hydride condition during its first absorption. Further hydriding processes closely resemble the behavior shown for the activated absorption stage.

We have performed SEM observations of samples corresponding to all the alloys under study after 3 hydrogen absorption/desorption pressure cycles. Images shown in Fig. 3 correspond to alloy Sn02, but the main features were also observed in all other samples. Fig. 3(a) is a low magnification image showing a general view of the activated material. As a result of the activation process, the mean particle size went from about 2 mm to 20 μm. Some relatively large chunks of material can still be seen in the picture with a size around 150 μm. Fig. 3(b) is a close up on the central part of the area shown in Fig. 3(a), which includes one of these bigger particles. Most of the particles in the image have well defined edges and smooth faces, which suggests they were formed by brittle fracture from larger pieces. Fig. 3(c) shows a detail of the surface of the large particle at the center of Fig. 3(b). Two important features can be observed in this figure. First, what appears as a big particle at low magnification (see the center area of Fig. 3(b)), is actually severely cracked. The bigger particle is composed of smaller pieces with a size in the micrometer range. This is a classic feature observed in AB_5 materials in the as-activated state and it is usually associated to the generation of fresh surface during activation.

In this sense, the evidence of this early decrepitation process can be related to the fast activation process observed in $LaNi_{5-x}Sn_x$ alloys (Fig. 2). The second important feature visible in Fig. 3(c) is the presence of cleavage lines on the surface. The lines follow two well defined directions in most of the pieces and form a step-like pattern. The presence of these marks provides additional evidence of the brittle character of the fracture process that gave place to these particles.

3.3. *Pressure–composition isotherms*

Fig. 4(a) and (b) shows examples of the absorption branch of dynamic PCT measurements at different temperatures for alloys Sn01 and Sn05, respectively. These results illustrate the behavior of materials with relatively low and high Sn content. The graphs show that a small amount of hydrogen is incorporated to the system at the beginning of the measurements, up to about 0.05 wt.% H, at very low pressure (up to 30 kPa). The dynamic measurement procedure used in this work essentially integrates the incoming hydrogen flux as detected by a calibrated flow controller. Similar experiments performed with an empty reactor using the same procedure do not show this kind of signal, so it does not seem to be an experimental artifact. As these initial parts do not play a role on the thermodynamic data extracted from the measurements, they were left as measured although we still cannot provide a clear physical explanation about their origin.

In the case of alloy Sn01 (Fig. 4(a)), the dynamic equilibrium pressure increases from 189 kPa at 300 K up to 2530 kPa at 410 K. As a result, the equilibrium pressure increases about 13 times for 110 K temperature difference. On the other hand, alloy Sn05 has a dynamic equilibrium pressure of 8.5 kPa at room temperature, and a corresponding equilibrium pressure

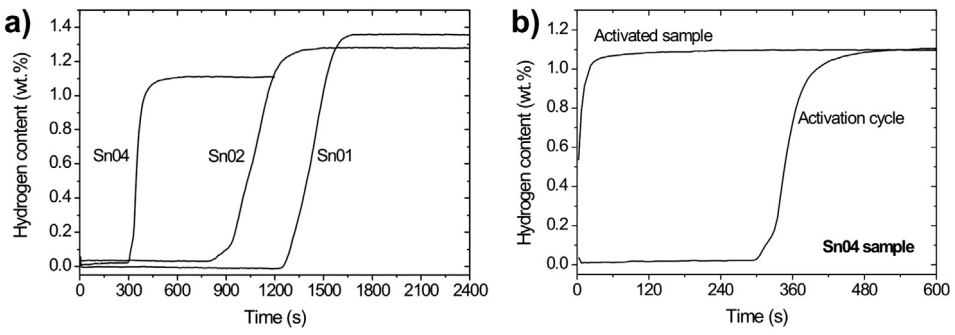

Fig. 2 – (a) Hydrogen intake as a function of time for the activation stages of samples containing Sn. (b) Comparison between the first activation stage and the fourth hydriding stage for a Sn04 sample.

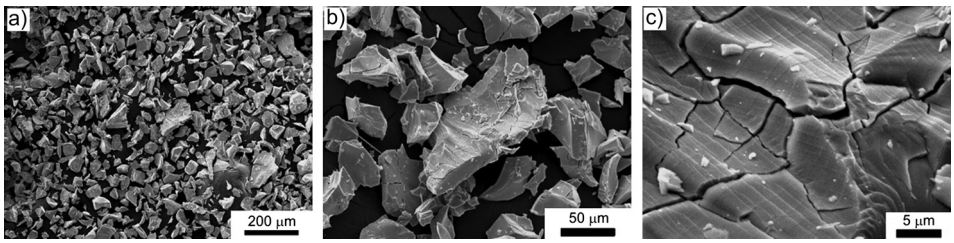

Fig. 3 – SEM pictures of sample Sn02 after 3 activation cycles. (a) General view. The material is distributed in particles with sizes around 20 μm (b) Close up of the central area of picture 3a. Particles show sharp edges and apparent cracking. (c) Central area of picture 3b, as seen with higher magnification. Particles are heavily cracked. Resulting pieces have sizes ranging from 1 μm to 5 μm. Cleavage lines are also apparent on the surface of the particle.

ratio over 30:1 at 410 K. This ratio is very high compared to other AB_5 alloys. From the point of view of applications, this particular alloy can absorb hydrogen below ambient pressure at room temperature, while desorption pressure could be as high as 270 kPa if the temperature were increased by 110 K.

Fig. 5(a) presents dynamic absorption isotherms measured at 355 K for the alloys under study. Fig. 5(b) shows the results corresponding to the absorption isotherms of all samples under study at different temperatures. The equilibrium pressure and hydrogen storage capacity decrease with the increment of Sn amount in the alloy, both in agreement with previous reports [14,23,29]. The results show a linear trend between the pressure logarithm and Sn content, reflecting the linear dependence found between the reaction enthalpy and amount of Sn. The main outcome of present results is that the dynamic equilibrium pressure at room temperature can be selected in a wide interval from 250 kPa to 8.5 kPa, simply by controlling the Sn concentration in the material. This feature is useful from the point of view of applications because it allows tailoring the material reaction with hydrogen in order to meet specific design requirements.

Fig. 6(a) and (b) are Van't Hoff plots presenting the dynamic equilibrium pressure measurements for the whole set of alloys as a function of temperature for hydrogen absorption and desorption, respectively. Dynamic equilibrium pressures were evaluated at the center of the plateau for each sample. Remarkably, all studied alloys containing Sn reacted with hydrogen at pressures below atmospheric pressure at room temperature. Individual data sets can be fit using the Van't Hoff expression:

$$R\ln P = \Delta H/T + \Delta S \quad (1)$$

Here, R is the ideal gas constant, P is the dynamic equilibrium pressure, ΔH is the reaction enthalpy, T is the temperature and ΔS is the entropy change. Applying Eq. (1) to experimental data sets, we have obtained the values presented in Table 2.

Although Luo and coworkers pointed out that isotherms measured at temperatures above 300 K are less reliable for precise determination of enthalpy and entropy values [24], those obtained in this work are in agreement with their results [14] within the margin of experimental error. Entropy values show a larger dispersion than values obtained by Luo et al. [14], as shown in Fig. 7(a). A linear fit of current data is included in Fig. 7(a) to show that values are independent of Sn content. The mean value obtained, $\Delta S = 104$ J/mol K, is slightly lower than the value of $\Delta S = 108$ J/mol K reported in [14] as the average of several samples. The estimated error margin for this latter average would be at least of ± 4 J/mol K [14]. It should also be noted that while Luo et al. defined the equilibrium pressure as that taken at a fixed hydrogen content ($H/AB_5 = 3$) for all temperatures and samples, we decided to use the standard criterion of taking the equilibrium pressure as that corresponding to the middle of the plateau. This criterion leads to consistently lower pressure values. As a result, present entropy values are lower than those reported in [14] but still within the margin of experimental error.

Enthalpy values presented in Table 2 are plotted in Fig. 7(b) together with those values reported by Luo et al. [14]. The enthalpy linearly increases with the increment in Sn content. A similar trend was previously informed in [14]. Present results are within the margin of error with respect to those literature values, although showing a larger difference between absorption and desorption. This effect is probably related to the dynamic nature of the measurement technique which involves a certain degree of indetermination in the sample temperature.

Hysteresis values are calculated using the following expression [30]:

$$\mathrm{Hys}_T = 1/2RT\ln\left(P_a/P_d\right) \quad (2)$$

, where P_a and P_d are the hydrogen absorption and desorption equilibrium pressures, respectively. Hysteresis values presented in Table 2 were calculated for $T = 355$ K. Present hysteresis values are higher than those reported by Luo et al. [14]. This difference can be rationalized by considering the dynamic character of present absorption/desorption measurements.

Hysteresis values are lower for alloys containing Sn than for $LaNi_5$. Considering the Van't Hoff expression (1), hysteresis in hydride forming systems can be related to an enthalpy difference between the hydrogen absorption and desorption stages. The corresponding energy difference is, at least in part, available to produce the plastic deformation in the material that accommodates the volume difference between the metal and hydride phases [19,31,32]. In the case of $LaNi_5$ the internal stresses involved in the phase transformation are very high, stabilizing an intermediate β phase [33] that has not been observed in $LaNi_{5-x}Sn_x$ alloys [15,34]. Fultz et al. [29] have

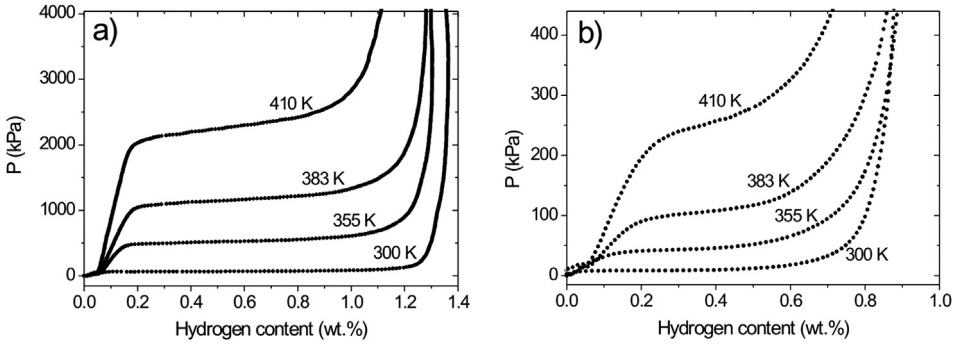

Fig. 4 – Absorption branch of dynamic PCT measurements at different temperatures for alloys: (a) Sn01 and (b) Sn05.

shown that during the hydriding process, internal hydrogen distribution is more homogeneous for the ternary alloys containing Sn than in $LaNi_5$. As a consequence, internal stresses are expected to be lower in ternary alloys, which would explain the fact that vacancy formation is two orders of magnitude lower in these alloys compared to $LaNi_5$ [35].

3.4. *Reaction kinetics*

Fig. 8(a) and (b) shows the results from reaction kinetics measurements at 316 K in the absorption and desorption stages, respectively. These results can be regarded as operational information, for all samples were measured under the same initial pressure and temperature conditions. During the absorption stage the initial pressure was set at 750 kPa and the resulting final pressure was around 630 kPa for all samples. Absorption kinetics improve with the addition of Sn, mainly due to the increased driving force resulting from the difference between the external initial pressure and the equilibrium pressure for each case. All Sn containing alloys are hydrided after 60 s. In particular, alloys Sn04 and Sn05 are completely hydrided after 30 s.

In the case of desorption measurements the pressure was kept below 5 kPa by evacuating an intermediate volume when necessary. This procedure introduces a slight but visible ripple in the curves corresponding to alloys with higher Sn contents, due to their lower equilibrium pressure. Desorption kinetics decrease as the amount of Sn in the alloys increases. Once again, this observation is associated to the driving force difference resulting from the externally set pressure and each alloy equilibrium pressure.

Laurencelle et al. [16] analyzed kinetic results in terms of a shrinking plate model characterized by an exponential dependence of the type $x_r = (1 - e^{-kt})$, where x_r corresponds to the reacted fraction, k is the kinetic coefficient and t is the elapsed time. After Ron [36], the kinetic coefficient depends on the temperature (T) and the initial pressure (P), and it can be expressed in terms of an activation energy E_a, a reaction rate constant k_0 and the equilibrium pressure measured at the middle of the reaction plateau ($P_{1/2}$) at the same temperature:

$$k = k_0 \left| \frac{P - P_{1/2}}{P_{1/2}} \right| e^{\frac{E_a}{RT}} \tag{3}$$

Values for k reported by Laurencelle et al. were determined directly from the kinetic curves by measuring the time at which half the material had reacted with hydrogen ($t_{1/2}$) and then using the relation: $k = \ln(2)/t_{1/2}$. A similar procedure was applied to present results in order to calculate k coefficients for each alloy (Table 3). Although a shrinking plate model could be an over simplification, we can compare current results to those reported by Laurencelle et al. for a $LaNi_{4.8}Sn_{0.2}$ alloy [16]. Alloy Sn01 will be used as a basis for the comparison as it has a similar chemical composition to the reported material. Measured values cannot be directly compared because

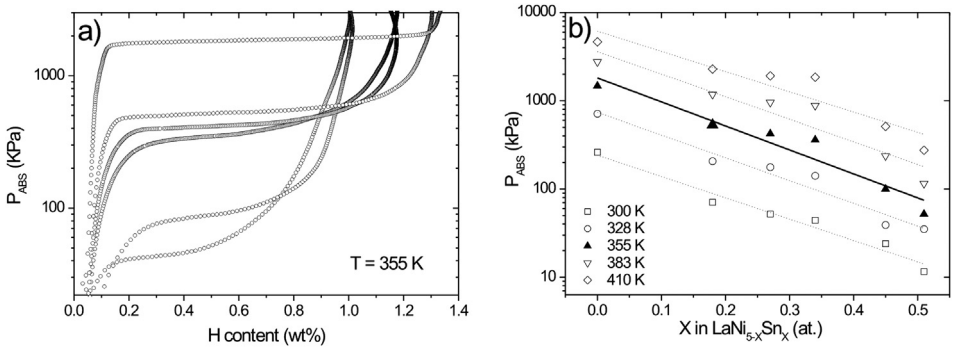

Fig. 5 – (a) Dynamic hydrogen absorption isotherms at 355 K corresponding to all the alloys studied in this work. (b) Dynamic equilibrium pressure as a function of the Sn content of $LaNi_{5-x}Sn_x$ alloys at different temperatures. Lines have been added as a guide to the eye. Solid line and symbols correspond to the curves shown in (a).

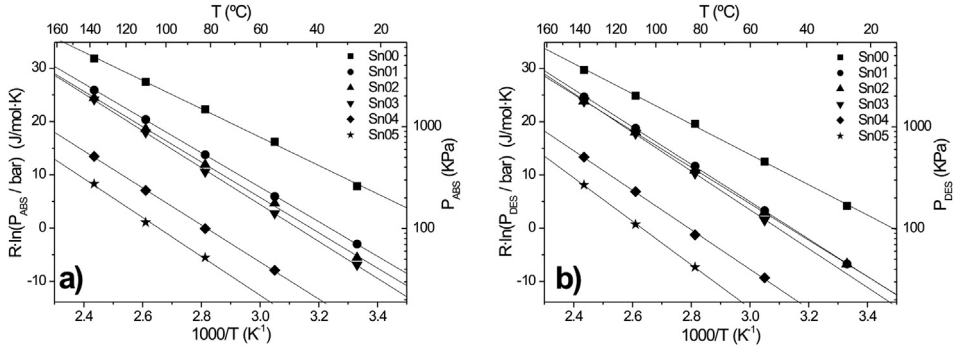

Fig. 6 – Van't Hoff plots of measured dynamic equilibrium pressures as a function of the temperature for $LaNi_{5-x}Sn_x$ alloys. Black symbols are measured values and lines represent the corresponding least-squares linear fits using Eq. (1). (a) Hydrogen absorption results. (b) Hydrogen desorption results.

Table 2 – Reaction enthalpy (ΔH), entropy change (ΔS) corresponding to hydrogen absorption (ABS) and desorption (DES) processes, and reaction hysteresis (Hys) for $LaNi_{5-x}Sn_x$.

Alloy	ΔH_{ABS} (kJ/mol H_2)	ΔS_{ABS} (J/K mol H_2)	ΔH_{DES} (kJ/mol H_2)	ΔS_{DES} (J/K mol H_2)	$Hys_{355\ K}$ (J/mol H_2)
Sn00	29 ± 2	107 ± 7	32 ± 2	114 ± 7	438
Sn01	32 ± 2	105 ± 7	35 ± 2	110 ± 7	362
Sn02	33 ± 2	105 ± 7	34 ± 2	107 ± 7	173
Sn03	35 ± 3	108 ± 10	37 ± 5	113 ± 15	334
Sn04	34 ± 3	98 ± 9	37 ± 3	104 ± 9	197
Sn05	36 ± 5	97 ± 13	40 ± 5	107 ± 15	302

Laurencelle et al. applied in absorption an initial hydrogen pressure of 340 kPa while, for a similar alloy, we applied 750 kPa. In desorption they used 10 kPa while 5 kPa were applied in this work. However, by using Eq. (3) and the values reported by Laurencelle et al. for E_a, k_0 and $P_{1/2}$ in absorption and desorption, results can still be compared. Table 3 includes k values calculated from Laurencelle et al. results for 313 K and 750 kPa in absorption, and 5 kPa in desorption.

In the case of the absorption stage, the current value for k_{abs} is close to that calculated from Laurencelle et al. fits of their kinetic results. However, the desorption kinetics reported here is considerably faster. A possible explanation for this difference resides in the different procedure necessary for performing kinetic measurements in absorption and desorption. In one hand, the absorption stage kinetic measurements can be performed essentially in one step by placing enough hydrogen to completely hydride the sample inside the reactor. On the other hand, during desorption the pressure increased abruptly at the beginning as the samples release hydrogen. This sudden increase affects the desorption kinetics as the reactor free volume is filled with hydrogen, and it coincides with the part of the desorption curves from where k_{des} values are determined. As we used a lower initial pressure, and considering similar reactors and sample sizes, this could

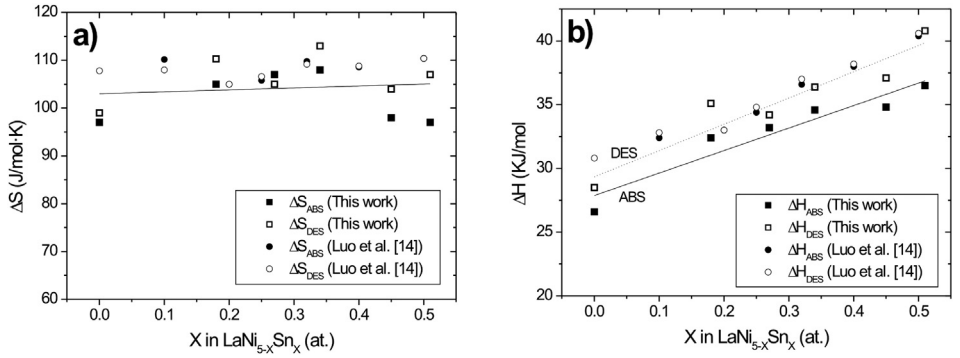

Fig. 7 – (a) Entropy values versus Sn content, calculated from Van't Hoff plots according to Eq. (1). The line corresponds to a linear fit of the data. Values from Luo et al. [14] have been included for comparison. (b) Enthalpy values versus Sn content, calculated from Van't Hoff plots according to Eq. (1). The solid and dotted lines correspond to linear fits of absorption and desorption data, respectively. Values from Luo et al. [14] have been included for comparison.

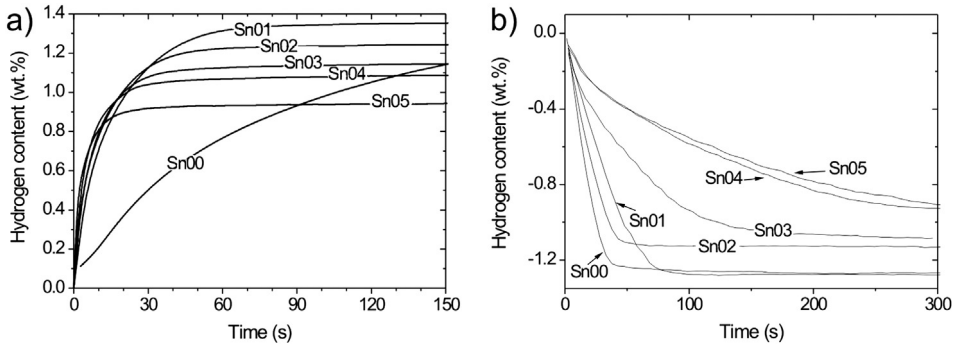

Fig. 8 – Reaction kinetics measurements for $LaNi_{5-x}Sn_x$ alloys at 316 K (a) Hydrogen absorption stage. Initial pressure: 750 kPa (b) Hydrogen desorption. External pressure: 5 kPa. Ripple in desorption curves arises from the experimental method (see text).

Table 3 – Kinetic coefficients under absorption (k_{abs}) and desorption (k_{des}) calculated from present results. The temperature is 316 K, and external pressure corresponds to 750 kPa in absorption and 5 kPa in desorption. In the case of alloy Sn01, values calculated from Laurencelle et al. results corresponding to $LaNi_{4.8}Sn_{0.2}$ alloy at 313 K [16] are included for comparison.

Alloy	k_{abs} (s^{-1})	k_{des} (s^{-1})
Sn00	0.014	0.046
Sn01		
This work	0.055	0.023
Laurencelle [16]	0.044	0.011
Sn02	0.092	0.036
Sn03	0.102	0.008
Sn04	0.125	0.003
Sn05	0.279	0.003

explain the observed difference. In addition, and by following a similar argument, current k_{des} values for the samples containing higher amounts of Sn (Sn04 and Sn05) are probably affected by the measurement procedure and should be regarded as approximate.

An improvement in the reaction kinetics due to the introduction of Sn in place of Ni is expected to result from the deformation associated to the lattice expansion produced by Sn (Fig. 1) and its positive influence on H_2 diffusion on the material surface and in the bulk [37,38]. However, under fixed initial pressure conditions such as those used in this work the dominant effect is given by the driving force associated to the pressure difference, which is larger for higher substituted alloys in absorption and the opposite in desorption. Quantification of the effect of the different mechanisms responsible for the observed kinetics needs further examination and is the subject of ongoing research.

4. Conclusions

$LaNi_{5-x}Sn_x$ alloys with $0 \leq x \leq 0.5$ were successfully prepared by arc melting and their structure and microstructure characterized by means of X-ray diffraction and SEM observations. Sn containing alloys readily reacted with hydrogen after a single step activation process. Dynamic equilibrium absorption and desorption pressures were measured. The substitution of Ni by Sn results in a lower equilibrium pressure. Moreover, absorption kinetics is increased by increasing the amount of Sn in the material. This last effect is partially related with the increased driving force related to the difference between the external pressure and the equilibrium pressure. Research is being performed to identify the kinetics determining mechanism. From the point of view of applications in hydrogen sequestration systems, alloys containing Sn in the range $0.2 \leq x \leq 0.4$ are good candidates for their use in devices due to their low dynamic equilibrium pressure and fast hydrogen absorption kinetics. The actual selection will probably be limited by desorption kinetics and the final pressure reached by the hydrogen evacuation system.

Acknowledgments

The authors acknowledge the help of S. Rivas, F. Roldán, E. Aburto and M. Isla for their help in the preparation of samples and the construction of hydrogen characterization equipment. C. Osuna helped with alloys chemical analysis. This work has been supported by ANPCyT (PAE 36985, PAE-PICT 2007-00158) and by ANPCyT-CNEA through fellowships from PFDT-PRH 200.

REFERENCES

[1] Sandrock G. A panoramic overview of hydrogen storage alloys from a gas reaction point of view. J Alloys Compd 1999;293–295:877–88.
[2] Dantzer P. Properties of intermetallic compounds suitable for hydrogen storage applications. Mater Sci Eng A 2002;329–331:313–20.
[3] Sakintuna B, Lamari-Darkrim F, Hirscher M. Metal hydride materials for solid hydrogen storage: a review. Int J Hydrogen Energy 2007;32:1121–40.
[4] Goodell PD. Stability of rechargeable hydriding alloys during extended cycling. J Less-Common Met 1984;99:1–14.

[5] Joubert J-M, Latroche M, Černý R, Percheron-Guégan A, Yvon K. Hydrogen cycling induced degradation in $LaNi_5$-type materials. J Alloys Compd 2002;330–332:208–14.

[6] Meyer G, Arneodo Larochette P, Baruj A, Castro FJ, Lacharmoise P, Zacur E, et al. Equipment for hydrogen absorption-desorption cycling characterization of hydride forming materials. Rev Sci Instrum 2007;78. art. 023903.

[7] Cohen RL, West KW. Intrinsic cycling degradation in $LaNi_5$ and annealing procedures for re-forming the material. J Less-Common Met 1983;95:17–23.

[8] Mendelsohn MH, Gruen DM, Dwight AE. $LaNi_{5-x}Al_x$ is a versatile alloy system for metal hydride applications. Nature 1977;269:45–7.

[9] Percheron-Guégan A, Lartigue C, Achard JC. Correlations between the structural properties, the stability and the hydrogen content of substituted $LaNi_5$ compounds. J Less-Common Met 1985;109:287–309.

[10] Iosub V, Latroche M, Joubert JM, Percheron-Guégan A. Optimisation of $MmNi_{5-x}Sn_x$ (Mm = La, Ce, Nd and Pr, $0.27 < x < 0.5$) compositions as hydrogen storage materials. Int J Hydrogen Energy 2006;31:101–8.

[11] Clay KR, Goudy AJ, Schweibenz RG, Zarynow A. The effect of the partial replacement of lanthanum in $LaNi_5H$ with cerium, praseodymium, and neodymium on absorption and desorption kinetics. J Less-Common Met 1990;166:153–62.

[12] Wang B, Chen Y, Liu Y. Structure and electrochemical properties of $(La_{1-x}Dy_x)_{0.8}Mg_{0.2}Ni_{3.4}Al_{0.1}$ ($x = 0.0$–0.20) hydrogen storage alloys. Int J Hydrogen Energy 2012;37:9082–7.

[13] Lambert SW, Chandra D, Cathey WN, Lynch FE, Bowman Jr RC. Investigation of hydriding properties of $LaNi_{4.8}Sn_{0.2}$, $LaNi_{4.27}Sn_{0.24}$ and $La_{0.9}Gd_{0.1}Ni_5$ after thermal cycling and aging. J Alloys Compd 1992;187:113–35.

[14] Luo S, Luo W, Clewley JD, Flanagan TB, Wade LA. Thermodynamic studies of the $LaNi_{5-x}Sn_x$-H system from $x = 0$ to 0.5. J Alloys Compd 1995;231:467–72.

[15] Luo S, Clewley JD, Flanagan TB, Bowman Jr RC, Cantrell JS. Split plateaux in the $LaNi_5 - H$ system and the effect of Sn substitution on splitting. J Alloys Compd 1997;253–254:226–31.

[16] Laurencelle F, Dehouche Z, Goyette J. Hydrogen sorption cycling performance of $LaNi_{4.8}Sn_{0.2}$. J Alloys Compd 2006;424:266–71.

[17] Cantrell JS, Beiter TA, Bowman Jr RC. Crystal structure and hydriding behavior of $LaNi_{5-y}Sn_y$. J Alloys Compd 1994;207–208:372–6.

[18] Joubert JM, Latroche M, Černý R, Bowman Jr RC, Percheron-Guégan A, Yvon K. Crystallographic study of $LaNi_{5-x}Sn_x$ ($0.2 \leq x \leq 0.5$) compounds and their hydrides. J Alloys Compd 1999;293–295:124–9.

[19] Matsuda J, Nakamura Y, Akiba E. Lattice defects introduced into $LaNi_5$-based alloys during hydrogen absorption/desorption cycling. J Alloys Compd 2011;509:7498–503.

[20] Nakamura Y, Bowman Jr RC, Akiba E. Variation of hydrogen occupation in $LaNi_{4.78}Sn_{0.22}D_x$ along the P–C isotherms studied by *in situ* neutron powder diffraction. J Alloys Compd 2007;431:148–54.

[21] Mendelsohn MH, Gruen DM, Dwight AE. The effect on hydrogen decomposition pressures of group IIIa and IVa element substitutions for Ni in $LaNi_5$ alloys. Mater Res Bull 1978;13:1221–4.

[22] Sato M, Yartys VA. Hydrogen absorption–desorption characteristics of the $LaNi_5Sn$ intermetallic compound. J Alloys Compd 2004;373:161–6.

[23] Luo S, Clewley JD, Flanagan TB, Bowman Jr RC, Wade LA. Further studies of the isotherms of $LaNi_{5-x}Sn_x - H$ for $x = 0$–0.5. J Alloys Compd 1998;267:171–81.

[24] Sato M, Stange M, Yartys VA. Desorption behaviour of hydrogen in the $LaNi_{4.7}Sn_{0.3}$-H system. J Alloys Compd 2005;396:197–201.

[25] Meyer G, Rodríguez D, Castro F, Fernández G. Automatic device for precise characterization of hydride forming materials. In: Proceedings of the 11th World hydrogen energy conference, vol. 2, International Association for Hydrogen Energy. Stuttgart, Germany: Elsevier; 1996. p. 1293–8.

[26] Bielmann M, Kato S, Mauron P, Borgschulte A, Züttel A. Characterization of hydrogen storage materials by means of pressure concentration isotherms based on the mass flow method. Rev Sci Instrum 2009;80. art. 083901.

[27] Wasz ML, Desch PB, Schwarz RB. The effect of tin alloying on the structure of $LaNi_5$. Philos Mag A 1996;74:15–22.

[28] Shan X, Payer JH, Wainright JS. Improved durability of hydrogen storage alloys. J Alloys Compd 2005;430:262–8.

[29] Fultz B, Witham CK, Udovic TJ. Distributions of hydrogen and strains in $LaNi_5$ and $LaNi_{4.75}Sn_{0.25}$. J Alloys Compd 2002;335:165–75.

[30] Flanagan TB, Oates WA. Some thermodynamic aspects of metal hydrogen systems. J Alloys Compd 2005;404–406:16–23.

[31] Flanagan TB, Clewley JD. Hysteresis in metal hydrides. J Less-Common Met 1982;83:127–41.

[32] Balasubramaniam R. Hysteresis in metal-hydrogen systems. J Alloys Compd 1997;253–254:203–6.

[33] Shilov AL, Kost ME, Kusnetsov NT. The system $LaNi_5H_2$. J Less-Common Met 1988;144:23–30.

[34] Bowman Jr RC, Luo CH, Ahn CC, Witham CK, Fultz B. The effect of tin on the degradation of $LaNi_{5-y}Sn_y$ metal hydrides during thermal cycling. J Alloys Compd 1995;217:185–92.

[35] Sakaki K, Date R, Mizuno M, Araki H, Nakamura Y, Shirai Y, et al. Behavior of vacancy formation and recovery during hydrogenation cycles in $LaNi_{4.93}Sn_{0.27}$. J Alloys Compd 2009;477:205–11.

[36] Ron M. The normalized pressure dependence method for the evaluation of kinetic rates of metal hydride formation/decomposition. J Alloys Compd 1999;283:178–91.

[37] Ratnakumar BV, Witham C, Bowman Jr RC, Hightower A, Fultz B. Electrochemical studies on $LaNi_{5-x}Sn_x$ metal hydride alloys. J Electrochem Soc 1996;143:2578–83.

[38] Sato M, Uchida H, Stange M, Yartys VA, Kato S, Ishibashi Y, et al. H_2 reactivity on the surface of $LaNi_{4.7}Sn_{0.3}$. J Alloys Compd 2005;402:219–23.